Microsolvation of Hot Ions: Spectroscopy and Statistical Mechanics of Phenide-Water Interactions

Beverly Feng [a] and Andrei Sanov [a,*]

[a] Department of Chemistry and Biochemistry, The University of Arizona, Tucson, Arizona 85721, United States

* Email: sanov@arizona.edu

ABSTRACT

Thermal excitation alters the spectroscopic signatures of solvated ions and affects their interactions with neighboring molecules. By analyzing the photoelectron spectra of microhydrated phenide (Ph^-), the temperatures of the $Ph^-{\cdot}H_2O$ and $Ph^-{\cdot}(H_2O)_2$ clusters from a hot ion source were determined to be 560 K and 520 K, respectively, vs. 700 K for unsolvated Ph^-. Compared to theory predictions for cold clusters, high temperature of the environment significantly reduces the average hydration stabilization of the ions and the corresponding band shifts in their spectra. The results are discussed in terms of a statistical model that describes the energy content of the intermolecular (IM) degrees of freedom of the cluster, $\langle E_{IM} \rangle$. We show that over the entire solvation energy range, the density of states associated with the IM modes of $Ph^-{\cdot}H_2O$, of which there are only 6, is more than an order of magnitude greater than that associated with the 27 internal vibrations of the core anion. The results suggest that the observed cluster temperatures are not determined by the ion source but represent the intrinsic properties of the clusters. The energetics and statistical mechanics of microsolvation limit the excitation that the IM degrees of freedom can sustain without significant solvent evaporation on the timescale of the experiment. The limit is expressed as a characteristic solvation temperature (CST), which is the maximum canonical temperature of a stable cluster ensemble. Driven by evaporative cooling, the terminal cluster temperature from a hot ion source will always be close to the cluster's CST. Only if the source temperature is lower than CST will the observed cluster temperature be determined by the source conditions. An approximate rule is proposed for estimating the characteristic temperature of any cluster using the inflection point on the $\langle E_{IM} \rangle$ vs. T curve.

1. Introduction

Spectroscopists love working with cold molecules because low temperatures limit the number of observed transitions and simplify spectral modeling. But our world and the Universe are not uniformly cold. High temperatures are encountered in many diverse environments, such as plasmas, exothermic reaction systems, stellar and planetary atmospheres, to name a few. It is, therefore, important to consider the effects of thermal excitation on the spectroscopic signatures and chemical properties of compounds.

Here, we report on the interactions of hot phenide (deprotonated benzene, $C_6H_5^-$) with water. Phenide (Ph^-) photodetachment yields the phenyl radical, which serves as an intermediate in the formation of polycyclic aromatic hydrocarbons[1-3] and is thus involved in many environmental processes.[4-5] The photoelectron spectroscopy of relatively cold (~300 K) phenide was studied by Lineberger and co-workers,[6] but the absorption spectra of polyatomic species can change significantly even at a moderately elevated temperature. In our recent work,[7] we examined phenide's spectroscopy at ~700 K and showed that already just above 300 K (hardly an extreme environment), the majority of Ph^- is promoted to vibrationally excited states. Such population shift leads to congested spectra, consisting primarily of hot bands. The highly averaged spectral shapes observed in this regime are controlled by the vibrational partition function,[8-10] while the properties of the ground state,[6,11] including its Franck-Condon (FC) profile,[12-14] become less relevant. Importantly, these thermally induced changes diminish the practicality of state-specific calculations and necessitate an alternative, statistical approach to spectral modeling.[7]

Thermal excitation also affects the intermolecular (IM) interactions in solvated and reactive environments. In the present work, we investigate the microhydration interactions in, specifically, hot $Ph^-\cdot(H_2O)_{1,2}$ clusters, but many of our conclusions are quite general. Building on the recent study[7] of hot unsolvated Ph^-, we consider energy partitioning among the molecular and intermolecular degrees of freedom and determine the factors controlling the cluster temperature.

At the outset, it is useful to examine how the vibrational partition function or, equivalently, its inverse Laplace transform—the density of states (DOS)—of $Ph^-\cdot H_2O$ differs from that of Ph^-. For that, we turn to Figure 1, which compares the vibrational DOS of Ph^- (black symbols) to the DOS associated with only the phenide-water IM degrees of freedom in the $Ph^-\cdot H_2O$ cluster (red symbols). The upper limit of the excitation range in these calculations corresponds to the $Ph^-\cdot H_2O \rightarrow$

$Ph^- + H_2O$ dissociation limit, excluding the zero-point vibrational energy (ZPE) in each case. The computational details and the meaning of the third curve (blue symbols) will be discussed later. For now, it is striking that over the entire energy range of interest, the DOS associated with the IM modes, of which there are only 6, is more than an order of magnitude greater than that associated with the 27 internal vibrations of the core anion, Ph^-. Given that the lowest IM frequency is almost 10 times smaller than that among the Ph^- modes, this observation should not be surprising. It does, however, indicate that the cluster's statistical properties are dominated by the inter- rather than intra-molecular motions. Put in another way, a 0.5 eV excitation of $Ph^-\cdot H_2O$ gives access to 24,867 internal states of Ph^-, compared to 248,525 distinct phenide-water interaction states.

The IM degrees of freedom also control how much thermal excitation the cluster can sustain. Simply put, if at any time the IM excitation exceeds the solvent binding energy, the cluster will promptly dissociate. This has been used with great success in evaporative-cooling and, in particular, argon-tagging experiments, where a rare-gas solvent ensures that the cluster is cold and, moreover, can be used as a messenger of infrared predissociation to obtain the spectra of the cold tagged species.[15-22] Although this effect has not been utilized as much in photoelectron spectroscopy, our focus here is not evaporative cooling, but quite the opposite: we aim to study the spectroscopy and statistical mechanics of the microscopic interactions at the highest cluster temperature that can be achieved *despite* the cooling. That is why we choose water, not argon. The Ar-tagging method relies on the relative weakness of the solvation interactions with argon but is not limited to argon only.[23-24] In $Ph^-\cdot(H_2O)_n$, water too can be viewed as a "tag", but with a much larger binding energy. The relative strength of microhydration allows these clusters to remain stable at much higher temperatures without significant predissociation, but there is still a limit to how much thermal excitation the phenide-water interactions can sustain.

This limit is determined by the thermodynamics of solvation. Since it is a property of the interactions, we will refer to it as the characteristic solvation temperature (CST). Importantly, CST of a given cluster is a fixed property that should not be confused with the canonical temperature. We will show that for $Ph^-\cdot H_2O$, CST is approximately 560 K. The corresponding temperature, T = CST, is quite high by the standards of gas-phase spectroscopy (much higher than for an argon-tagged system). Therefore, the strongly solvated systems, such as $Ph^-\cdot H_2O$ allow, in practice, for two distinct cluster generation regimes, depending on the ion source conditions. In a "hot" source (source temperature > CST), the hot nascent cluster ions are cooled by solvent evaporation[25-30]

until their temperature reaches the CST. The terminal temperature of clusters generated in a hot ion source is thus determined by the microsolvation interactions rather than the intricacies of the source. Only in a cold source (source temperature < CST), will the observed cluster temperature be controlled by the specific source conditions.

2. Experimental Methods

The negative-ion photoelectron imaging spectrometer used in this study has been described elsewhere.[31-32] The key distinction compared to the instrument's original design is the ion source configuration:[33-35] to generate hot cluster ions, we used a stripped-down version of a conventional electron gun,[33] to which we refer as the electron cannon.[7,36]

The precursor benzeneselenol (C_6H_5SeH), kept at room temperature and containing traces of water, is carried by argon gas at a backing pressure of ~1.8 atm into a pulsed supersonic nozzle (General Valve Inc., Series 9). The nozzle is placed inside the ion source chamber (2×10^{-7}/4-5×10^{-5} torr base/operational pressure) and operated at a repetition rate of 20 or 50 Hz, matching that of the laser used in each measurement.

The electron cannon is positioned close to the nozzle, as described in the previous publication.[7] It produces a continuous spray of ~100 eV electrons thermionically emitted from a 1 mm wide thoria-coated iridium filament (e-Filaments, LLC) heated by a 4-5 A direct current. The emitted electrons intersect a large volume of the supersonic expansion, generating hot plasma. The electron bombardment occurs, on average, many nozzle diameters downstream from the expansion origin, leaving little room for collisional cooling of the nascent ions. Therefore, this source configuration generates ions with significantly higher internal temperatures compared to a traditional ion source, in which a collimated electron beam ionizes the precursor expansion close to its origin.[31,33]

A pulsed repeller plate extracts anions into a Wiley-McLaren[37] time-of-flight mass-spectrometer. At the end of the flight tube, the ion packets of interest (Ph^-, $Ph^-\cdot H_2O$, or $Ph^-\cdot(H_2O)_2$ are intersected by a pulsed nanosecond laser beam. Light of 532 nm and 355 nm is produced as a second and third harmonics, respectively, of a Spectra Physics Lab-130-50 Nd:YAG laser (50 Hz repetition rate). 611 nm pulses are generated using Rhodamine 640 in an ND6000 dye laser pumped by the second harmonic of the Surelite II-20 Nd:YAG laser (Continuum, Inc., 20 Hz repetition rate).

The electrons photodetached from the targeted ions are projected using a velocity-map[38] imaging[39-40] assembly[31] onto a 40 mm diameter position-sensitive dual microchannel-plate imaging

detector coupled to a P47 phosphor screen. The photoelectron images are captured using a charge-coupled device camera (Roper Scientific, Inc.). The photoelectron spectra are obtained from the images *via* an inverse Abel transformation[40] using the BASEX program.[41]

3. Results and Analysis

The photoelectron images of hot Ph^- and $Ph^-\cdot H_2O$ ions were recorded at 355 nm (3.49 eV), 532 nm (2.33 eV), and 611 nm (2.03 eV). The $Ph^-\cdot W_2$ clusters were studied at 355 and 532 nm wavelengths only. The Ph^- results were reported previously[7] and included here for comparison with the cluster data. All photoelectron images are assembled in Figure 2, where the left half of each image represents the raw data, while the right is the corresponding inverse Abel transformation. The laser polarization direction is vertical in the plane of all images, as indicated in the figure.

The energy spectra obtained from the images are shown in Figure 3, plotted in black. All spectra are plotted with respect to electron binding energy, eBE = $h\nu$ − eKE, where eKE is electron kinetic energy. The red and blue (for Ph^- only) traces in Figure 3 represent model simulations, which will be discussed shortly. All experimental spectra, apart from Ph^- at 355 nm, consist of a single broad electronic band, which corresponds to photodetachment transitions from the ground electronic state of the phenide anion to the ground electronic state of the neutral phenyl radical (σ-Ph). The 355 nm spectrum of Ph^- includes an additional higher-energy band, corresponding to the first excited state of phenyl (π-Ph). Both the σ-Ph and π-Ph bands in isolated hot Ph^- were discussed in detail previously.[7] Here we focus on the microhydration-induced changes within the σ-Ph transition and no further comment will be made about the π-Ph band. The immediately apparent hydration effects in the $Ph^-\cdot W_{1,2}$ spectra include the band shifts to larger eBEs and the slight narrowing of the $Ph^-\cdot(H_2O)_{1,2}$ bands compared to Ph^-.

As shown previously, the thermal excitation in the temperature range of these experiments and the rapidly increasing with energy density of states shift the maximum of the Ph^- energy distribution to highly excited vibrational levels.[7] As a result, the photoelectron spectra are dominated by hot bands. A complete FC analysis taking into account the thermal excitations of all 27 normal modes of Ph^-, including the combination bands, is not only impractical, but unnecessary. A statistical approach to hot-ion spectra is far more preferable in this scenario.[7] The additional degrees of freedom in phenide-water clusters complicate the FC analysis even further, making statistical

modeling the only practical way to analyze the photoelectron spectra.

To start, the blue spectrum in each Ph^- panel in Figure 3 represents the complete FC simulation of cold-ion photodetachment.[6-7,11] These simulations[7] are based on the FC factors calculated using ezFCF, part of the ezSpectra suite of programs developed by Gozem and Krylov.[42] The red traces in the same figure present a consistent model description of the complete $Ph^-\cdot(H_2O)_{0\text{-}2}$ dataset, based on limited FC calculations combined with the DOS analysis and Boltzmann statistics.

The common modeling approach that considers only the FC-active vibrational modes is not appropriate for a statistical analysis of hot ions because thermal excitations are not subject to FC selection rules. Both FC-active and inactive vibrations are thermally excited on an equal footing and contribute to the partition function of the anion. Previously, we described several statistical methods for modeling hot photoelectron spectra, which account for the excitations of all available modes.[7] The statistical methods include the FC-active + dark bath model, the FC-active + bright bath model, and the energy-conservation approach. The results vary depending on how the bath-mode couplings are treated, but the FC-active + bright bath and the energy-conservation models yield similar results consistent with the experiment. The red traces in Figure 3 and the following discussion are based on the energy-conservation approach.

The spectral modeling assumes that the microscopic hydration in $Ph^-\cdot H_2O$ and $Ph^-\cdot(H_2O)_2$ affects their photoelectron spectra in two ways. First, the cluster temperatures are generally different from Ph^-. Second, to account for the solvation-induced stabilization, the hydrated spectra are shifted to larger eBEs, compared to Ph^-. We refer to this as the hydration shift, HS. The different-wavelengths spectra of each species in Figure 3 are modeled in a consistent manner using the same T, HS, and the Wigner exponent (discussed below), because these are ion properties, independent of photon energy. Other model parameters are defined in Ref. 7, but the band shifts are the most noticeable and easily understood spectroscopic effect of hydration. Based on the spectral modeling, the addition of the first water molecule shifts the Ph^- bands by HS = 0.38 eV, while the second water adds another 0.25 eV, for a total 0.63 eV shift of the $Ph^-\cdot(H_2O)_2$ spectrum relative to Ph^-.

From the same model spectra, the Ph^- temperature was determined to be 700 K, while the $Ph^-\cdot H_2O$ and $Ph^-\cdot(H_2O)_2$ spectra are described by T = 560 K and 520 K, respectively. The reduced temperatures of the hydrated species are manifest in the slight narrowing of their spectral bands compared to Ph^-, while other thermal effects will be discussed in Section 4.

To account for the eKE-dependence of the electronic part of the photodetachment cross-section,[43-46] the vibrational envelope of each model spectrum in Figure 3 is scaled[7] by an appropriate Wigner-like[47] function ε^P, where $\varepsilon \equiv$ eKE = $h\nu$ – eBE. The Wigner exponent of P = ½ describes *s* wave emission in the limit of a zero or small dipole moment of the neutral residue. Smaller P values may be necessary for an *s* wave in a large-dipole field.[44,47-48]

In practice, the Wigner exponent controls how fast the spectral intensity rises from zero near the eBE = $h\nu$ (eKE = 0) limit (indicated by green arrows in Figure 3). All three Ph^- spectra are modeled with the standard Wigner value for an *s* wave, $P = 0.5$.[47] However, the square-root scaling does not match the low-eKE behavior of some of the other spectra. Most notably, to reproduce the step-like increase to the left of eBE = $h\nu$ in the 532 nm spectrum of $Ph^-\cdot(H_2O)_2$, the exponent had to be lowered to $P = 0.10$. A similar but less pronounced rise in the 611 nm $Ph^-\cdot H_2O$ spectrum required a less significant reduction in P, to 0.45. Since P is physically determined by the dipole moment of the neutral residue, the same P values were assumed for a given species at each wavelength studied. The P values, together with the temperature and hydration shifts used to model the spectra in Figure 3 are all summarized in Table 1.

4. Modeling and Discussion

4.1. *Ab initio* calculations. The electronic, geometric, and vibrational structures of the $Ph^-\cdot H_2O$ cluster were investigated at the coupled-cluster level of theory with single and double excitations (CCSD) using the aug-cc-pVDZ basis set. These calculations, which employed the Q-Chem 5.1 program package,[49] complement the recent analysis of Ph^- reported elsewhere.[7]

Phenide has a C_{2v} equilibrium structure shown in Figure 4a, with a closed-shell electron configuration.[6-7,11] The optimized geometry of $Ph^-\cdot H_2O$ corresponds to a C_s symmetry structure shown in Figure 4b. The water molecule is bonded to the anion with a single anionic hydrogen bond and lies in the plane perpendicular to that of phenide. A similar structure (not shown), also single-H bonded and of C_s symmetry but with the water in the phenide plane, is slightly less stable (by 0.012 eV) and corresponds to a transition state between the equivalent out-of-plane structures.

Figure 4 also shows the Hartree-Fock HOMOs of Ph^- and $Ph^-\cdot H_2O$, from which the electrons are ejected *via* the σ-Ph transition. The geometric details for Ph^- and $Ph^-\cdot H_2O$ are given in Supporting Information (SI), along with the harmonic vibrational frequencies of $Ph^-\cdot H_2O$, Ph^-, and

H_2O. Furthermore, the calculations predict that the dipole moment of neutral Ph at the optimized geometry of Ph^- is 0.88 Debye, while that of neutral $Ph{\cdot}H_2O$ at the geometry of $Ph^-{\cdot}H_2O$ is 3.33 Debye. Calculations on $Ph^-{\cdot}(H_2O)_2$ were not attempted, but its neutral dipole moment is expected to be larger yet. This dipole trend is qualitatively consistent with the changes in the Wigner exponent (Table 1) needed to model the photoelectron spectra of Ph^- and $Ph^-{\cdot}(H_2O)_{1,2}$ in Figure 3.

The effect of mono-hydration can be glimpsed from the calculations in two ways. Comparing the CCSD energies of the neutral and the anion, both determined at the optimized geometry of the anion, yields a vertical detachment energy (VDE) of 1.431 eV for Ph^- and 2.205 eV for $Ph^-{\cdot}H_2O$. These quantities, indicated in Figure 5, correspond to a hydration-induced VDE shift, $\Delta VDE = 0.774$ eV. This is about twice the spectral shift from Ph^- to $Ph^-{\cdot}H_2O$ (HS = 0.38 eV) observed in the hot-ion spectra in Figure 3. As discussed below, this discrepancy is not surprising because the VDE is a ground-state (cold-ion) property, yet our ions are not cold.

A more direct energetic effect of hydration is revealed by comparing the $Ph^-{\cdot}H_2O$ energy to the combined energy of non-interacting phenide and water (Figure 5). We will refer to the difference as the hydration energy, $E_{hyd} = E(Ph^-) + E(H_2O) - E(Ph^-{\cdot}H_2O)$. It is similar to, but strictly not the same as ΔVDE. The CCSD calculations predict $E_{hyd} = 0.849$ eV. This result overestimates the cluster stability due to the basis set superposition error, which is the effect of calculating the cluster energy with more basis functions than used for its building blocks. Although often ignored, this error can be significant, especially for weak interactions.[50] To correct for it, we calculated the Ph^- and H_2O energies using the same basis set as for $Ph^-{\cdot}H_2O$ (the counterpoise correction).[51] In the Ph^- calculation, ghost atoms for H_2O were added to the optimized phenide structure in the same positions as in the $Ph^-{\cdot}H_2O$ cluster, allowing for the Ph^- energy to be calculated without the water but with its basis functions in place. Similarly, the water energy was determined with the ghost-phenide functions included.

The corrected hydration energy, $E_{hyd} = 0.780$ eV (indicated in Figure 5), is a slight reduction from the above 0.849 eV result. It is similar to $\Delta VDE = 0.774$ eV, and the slight remaining difference is due to the neutral-state interactions. Note that the dashed lines in Figure 5 indicate the Ph + H_2O and $Ph{\cdot}H_2O$ energies at the optimized geometries of Ph^- + H_2O and $Ph^-{\cdot}H_2O$, respectively, not the relaxed neutral structures.

4.2. Statistical mechanics of microhydration. Spectral shifts reflect the ion stabilization in sol-

vated environments. Their correct interpretation is important because they are often used to determine the microscopic solvation energies. Here we discuss the role of thermal excitation to explain the significant difference between HS = 0.38 eV observed in the $Ph^-\cdot H_2O$ spectrum, on the one hand, and the calculated ΔVDE and E_{hyd} values (0.774 and 0.780 eV, respectively), on the other. The conclusions are then extended to $Ph^-\cdot(H_2O)_2$.

In general, the spectral shifts observed for hot clusters should not be expected to match the *ab initio* ΔVDE or E_{hyd} exactly. The last two properties describe the cluster in its ground state, while at 560 K (the $Ph^-\cdot H_2O$ temperature), most of Ph^- is in excited vibrational levels with an average excitation of 0.26 eV above phenide's ZPE.[7] The $Ph^-\cdot H_2O$ cluster has 3×14 – 6 = 36 vibrational modes. In addition to the 27 internal vibrations of phenide and three of water, there are six IM modes of the phenide-water relative motion. Compared to molecular vibrations, the IM modes have, on average, lower frequencies and are, therefore, more active at a finite temperature. Importantly, these modes are absent in isolated Ph^- and hence their associated average energy, $\langle E_{IM} \rangle$, must be accounted for when comparing the $Ph^-\cdot H_2O$ spectral shift, HS, to E_{hyd}. No such correction is necessary for the Ph^- internal excitation because these modes are included in the phenide FC envelope.[7]

From a dynamics point of view, both HS and E_{hyd} describe the cluster stabilization due to IM interactions. However, E_{hyd} is defined for the equilibrium $Ph^-\cdot H_2O$ structure, while the spectral shift HS results from thermally averaged interactions sampling a range of the IM coordinates. Even with no excitation, the zero-point motion along the IM modes samples a range of cluster geometries and the microhydration interactions must be corrected for the potential-energy part of the combined ZPE of these modes. In a thermally excited cluster, larger amplitude motions beyond the zero-point further reduce the mean stabilizing effect of hydration (Figure 5).

To estimate the magnitude of this reduction (ΔHS), we consider a canonical ensemble of six-dimensional oscillators representing the six IM modes. The 36 normal-mode frequencies of $Ph^-\cdot H_2O$ from the CCSD/aug-cc-pVDZ harmonic calculations are listed in Table S1 in SI alongside the frequencies of isolated Ph^- (27 modes) and H_2O (3 modes). The modes corresponding predominantly to the phenide-water motions are labeled IM1-IM6 and their coordinates are illustrated in Figure 6. Near the dissociation limit, IM1, IM2, and IM4 map onto the phenide-water relative translation, giving these modes a direct dissociative character. IM3, IM5, and IM6, on the

other hand, resemble hindered rotations. Among them, IM5 and IM6 strongly couple to the dissociation coordinates because the corresponding motions can flip the water's dipole from an attractive to a repulsive orientation relative to the Ph^- charge. Since large-amplitude motions along either of these modes lead to *prompt* predissociation, they can be described as prompt-predissociative. For brevity, we will refer to all five modes (directly dissociative IM1, IM2, and IM4 and prompt-predissociative IM5 and IM6) as simply "dissociative". Only one IM mode, IM3, can be described approximately as non-dissociative: at high excitation it becomes a spinning motion of water about the IM axis that largely preserves the IM bonding.

We model the dissociative modes as Morse oscillators with a dissociation energy equal to that of $Ph^-{\cdot}H_2O$ (E_{hyd} = 0.780 eV), while IM3 is treated in the harmonic (non-dissociative) approximation. The fundamental frequencies ν_i, i = 1–6, of the six oscillators are set to the IM1-6 mode frequencies from the CCSD calculations (they are included in Figure 6 and Table S1). The anharmonicity for each mode except IM3 is obtained as $\nu_i x_i = \nu_i^2/(4E_{hyd})$.

Next, we used the direct state count method, similar to the one described previously for the internal modes of phenide,[7] to calculate the density of states, $\rho(E_{IM})$, spanned by the six IM modes as a function of energy. The direct count in the six-dimensional IM subspace yielded 4,567,101 distinct vibrational states below the dissociation limit (E_{hyd}), including the zero-point level with a ZPE_{IM} = 0.123 eV. We then partitioned the E_{IM} energy range from 0 to E_{hyd} into 100 equal-width bins and counted the number of states within each bin. The DOS values were calculated by dividing the number of states within a bin by its width. The result is plotted in Figure 1 (red) vs. the IM excitation energy, $E_{IM} - ZPE_{IM}$. As discussed in the Introduction, a similar DOS function was also calculated for the 27-dimensional vibrational space of phenide, spanned by modes Ph1-27 (Table S1). These modes were treated in the harmonic approximation and the resulting DOS is plotted in Figure 1 (black) with respect to the corresponding excitation energy (excluding phenide's ZPE).

The IM-DOS function $\rho(E_{IM})$ allows us to calculate the properties of the statistical ensemble describing the six IM modes of $Ph^-{\cdot}H_2O$. The Boltzmann energy distribution relates to $\rho(E_{IM})$ as

$$P(E_{IM}) \propto \rho(E_{IM})\exp\left(-E_{IM}/k_BT\right) \quad (1)$$

The resulting binned distributions for T = 300 K, 560 K (the experimental temperature of $Ph^-{\cdot}H_2O$), 700 K (the experimental temperature of Ph^-), and 1000 K, are shown in Figure 7. The ensemble average of energy, $\langle E_{IM}\rangle$, where E_{IM} includes ZPE_{IM}, is calculated at any given temperature as

$$\langle E_{\mathrm{IM}} \rangle = \int_0^{E_{\mathrm{hyd}}} E_{\mathrm{IM}}\, P(E_{\mathrm{IM}}) \mathrm{d}E_{\mathrm{IM}} \tag{2}$$

The dependence of $\langle E_{\mathrm{IM}} \rangle$ on T is represented by the red curve in Figure 8.

In the classical (high-temperature) harmonic limit,[8,52] the equipartition theorem predicts $\langle E_{\mathrm{IM}} \rangle = 6k_BT$ (one k_BT per vibration). In the temperature range of the present experiments, the phenide-water IM motions are neither classical nor harmonic, but it is useful to compare the results to this limit, represented in Figure 8 by a dotted line. As expected, the quantum model significantly deviates from the classical expectation at low temperatures. As T increases, the red model curve gravitates toward the $6k_BT$ limit, but the ensemble never turns completely classical. Energy quantization remains important over the entire T range of interest, at least for the highest-frequency modes. The average energy content per mode may also deviate from k_BT due to the anharmonicity associated with the cluster dissociation limit.[53-54] For comparison, the dashed blue curve in Figure 8 was calculated by treating all IM modes in the harmonic approximation (i.e., no dissociation allowed). The role of the anharmonicity becomes particularly clear at $T > 600$ K, where the red solid curve begins to saturate and eventually drops below both the quantum (dashed) and classical (dotted) harmonic limits. This drop off is due to the finite number of bound states of a Morse oscillator and the existence of an E_{IM} maximum, $\max(E_{\mathrm{IM}}) = E_{\mathrm{hyd}}$.[54] We deliberately do not include the continuum states ($E_{\mathrm{IM}} > E_{\mathrm{hyd}}$) because they do not represent bound clusters.

4.3. IM excitation vs. the spectral shift. At the $Ph^-{\cdot}H_2O$ temperature of 560 K, the model predicts $\langle E_{\mathrm{IM}} \rangle = 0.333$ eV (Figure 8). The question now is how this estimate affects the photoelectron spectra. In the absence of thermal excitation, the $Ph^-{\cdot}H_2O$ spectrum would be shifted to larger eBE by $E_{\mathrm{hyd}} = 0.780$ eV (minus a ZPE correction), but in a thermally excited ensemble, the shift is partially offset by the amount of IM excitation (not accounted for in FC modelling) transferred to the emitted electron.

Since IM interactions in the neutral state are weak compared to the anionic solvation, they can be neglected (zero or constant potential energy). One the other hand, IM energy of a bound $Ph^-{\cdot}H_2O$ cluster consists of the kinetic and potential parts. Upon ejecting an electron, the kinetic energy (KE) part of $\langle E_{\mathrm{IM}} \rangle$ is retained by Ph + H_2O (the sudden approximation), while the potential energy (PE) is imparted on the departing electron. For a harmonic oscillator, $\langle \mathrm{PE} \rangle = \langle E \rangle/2$, where E = KE + PE is the oscillator's total energy (the virial theorem), but this simple relation does not

hold for a dissociative anharmonic potential[53] such as that describing the $Ph^{-}\cdot H_2O$ IM interactions. For a Morse potential (for example), $\langle PE\rangle \approx (1/2)\langle E\rangle$ in the ground state, but $\langle PE\rangle \rightarrow \langle E\rangle$ for excited states near the dissociation limit (see SI). To estimate the spectral shift, one must also consider the FC factors connecting a given anion state to the neutral continuum states with different KE_{IM} values.

The analysis summarized in SI shows that approximately 60% of $\langle E_{IM}\rangle = 0.333$ eV is transferred to the departing electron, translating into a thermal offset of the hydration shift $\Delta HS = 0.20$ eV. The other 40% (0.13 eV) are imparted on the neutral fragments. This neutral-state excitation is indicated in Figure 5 by a red dotted line above the black dashed line representing $Ph\cdot H_2O$. The observed hydration shift HS is therefore related to the purely electronic hydration energy via $E_{hyd} = HS + \Delta HS = 0.38$ eV + 0.20 eV = 0.58 eV.

The remaining discrepancy with the CCSD result, $E_{hyd} = 0.780$ eV, is attributed to a combination of factors, such as the neglect of neutral-state interactions, a computational uncertainty (rather small basis, no triples corrections), and/or a systematic error in the statistical modeling of the hot-ion spectra. We particularly point out one plausible issue: the underlying assumption of a thermal equilibrium among all molecular and IM modes in the cluster. In a contrarian case, an incomplete participation of the high-frequency Ph modes would cause the model to underestimate the temperature of the active vibrations, including the low-frequency IM modes. (If some modes do not contribute fully to energy storage, a larger fraction of excitation revealed in the spectra must be absorbed by the participating modes). A slightly higher IM temperature would result in both a larger $\langle E_{IM}\rangle$ and a larger fraction of it being imparted to the electron, increasing the predicted ΔHS offset. Non-equilibrium energy partitioning is beyond the scope of this work but may be addressed in the future.

4.4. Characteristic solvation temperature. The IM energy distributions in Figure 7 suggest that the temperature of $Ph^{-}\cdot H_2O$ (560 K) is not an arbitrary feature of the ion source but an intrinsic property of the phenide-water system, i.e., its characteristic solvation temperature, CST. The distributions at $T > 560$ K have non-negligible populations at the evaporation limit, $E_{IM} = E_{hyd}$. Any population above this limit leads to decomposition of the highest-energy clusters, i.e., evaporative cooling,[25-30] which will continue until the population at the evaporation limit becomes negligible.

To quantify this effect, it should be considered that only five of the six IM modes in $Ph^{-}\cdot H_2O$ are dissociative. The probability for sufficient evaporation energy to be stored in these modes is

determined in the five-dimensional subspace $IM^{(5)}$ spanned by the IM1-2 and IM4-6 modes only (Figure 6 and Table S1). The binned DOS calculated using the Morse-potential treatment of these modes, as described in Section 4.2, is plotted in Figure 1 (blue symbols). The corresponding energy distribution $P_5(E_{IM}^{(5)})$ at $T = 560$ K is shown in Figure 9 (blue symbols), where it is compared to the $P(E_{IM})$ distribution (all six IM modes) at the same temperature (black symbols).

Next, we calculate the fraction of the $Ph^-{\cdot}H_2O$ population possessing a total dissociative-mode energy in the top 1% of the evaporation energy, i.e., with $E_{IM}^{(5)}$ between $0.99E_{hyd}$ and E_{hyd}. We label this fraction $f_{1\%}$ and will, for brevity, refer to this arbitrarily defined population as "ready to evaporate" (RTE). The RTE fraction is related to the evaporation rate and, therefore, the lifetime of the thermally excited clusters. At a given temperature, $f_{1\%} = P_5(E_{hyd})\Delta E_{IM}^{(5)}$, where $\Delta E_{IM}^{(5)} = 0.01E_{hyd}$. For example, from the 560 K $IM^{(5)}$ distribution in Figure 9, $P_5(E_{hyd}) = 0.013$ eV^{-1}. Multiplying this by $0.01E_{hyd} = 0.0078$ eV gives $f_{1\%}(560\text{ K}) = 1.0\times10^{-4}$, meaning that 0.01% of $Ph^-{\cdot}H_2O$ clusters at 560 K are labeled as "ready to evaporate". This percentage increases seven-fold at 700 K and 50-fold (to 0.5%) at 1000 K.

The $f_{1\%}(T)$ function is plotted in Figure 10 in red. It shows that the RTE fraction is vanishingly small at low temperatures but rises rapidly above ~500 K. It is not a coincidence that the observed temperature of $Ph^-{\cdot}H_2O$, $T = 560$ K, is just above this onset. It is also not a coincidence that this T is close to the inflection point on the $\langle E_{IM}\rangle$ vs. T curve in Figure 8, whose origin, discussed in Section 4.2, is also the existence of the evaporation limit at the top of the E_{IM} range.

This brings us to the conclusion that the observed $Ph^-{\cdot}H_2O$ cluster temperature is determined not by the specifics of our ion source but by phenide's microhydration strength. In other words, the observed T is the upper bound of excitation that the IM interactions within the cluster can sustain, i.e., the cluster's CST. Due to the large density of excited IM states, the $Ph^-{\cdot}H_2O$ ensemble is noticeably unstable with respect to water evaporation above 560 K. In terms of k_BT, the phenide-water interaction energy, $E_{hyd} = 0.780$ eV, corresponds to a much higher temperature of 9050 K. But already at $T > 560$ K the dissociative energy distribution begins to spill over significantly the cluster fragmentation limit, leading to evaporative cooling.

In sum, we interpret the experimentally determined $Ph^-{\cdot}H_2O$ temperature of 560 K as follows. Our ion source generates ions that are hotter initially, as signaled by the Ph^- temperature of 700 K, but evaporative cooling lowers the cluster temperatures until the evaporation rate becomes

negligible on the time scale of the experiment. For $Ph^-{\cdot}H_2O$, this happens at 560 K.

4.5. Twice-hydrated clusters. The addition of a second water molecule in $Ph^-{\cdot}(H_2O)_2$ increases the number of IM degrees of freedom to 12. Beside the phenide-water interactions, the H_2O-H_2O bonding and three-body effects may become important. We will, however, limit our brief discussion of the twice-hydrated clusters to the assumption that the two waters bind to the core anion independently and that the evaporation energy of the first H_2O from $Ph^-{\cdot}(H_2O)_2$ is similar to that in $Ph^-{\cdot}H_2O$. Under this assumption, we can divide the vibrational space defined by the 12 IM modes in $Ph^-{\cdot}(H_2O)_2$ into two independent but equivalent six-dimensional subspaces, each describing a single phenide-water interaction. Each dissociative subspace, $IM_a^{(5)}$ and $IM_b^{(5)}$, includes five dissociative and one non-dissociative modes, and each is described by its own distribution $P_5(E_{IM}^{(5)})$ obtained in Section 4.4. The probability for at least one of the two phenide-water interactions in $Ph^-{\cdot}(H_2O)_2$ to possess energy between a given $E_{IM}^{(5)}$ and $E_{IM}^{(5)} + \Delta E_{IM}^{(5)}$ is then $2P_5(E_{IM}^{(5)})\Delta E_{IM}^{(5)}$. To clarify, this is not the same as the probability for the total dissociative energy shared between two phenide-water subsystems to fall in the stated range because $E_{IM}^{(5)}$ is the energy of one five-dimensional subspace only. It follows that the fraction of $Ph^-{\cdot}(H_2O)_2$ that is "ready to evaporate" at least one water is $2f_{1\%}$, where $f_{1\%}$ is the RTE fraction for $Ph^-{\cdot}H_2O$ (Section 4.4).

The RTE fraction for $Ph^-{\cdot}(H_2O)_2$ is represented by the blue curve in Figure 10, on the same graph as the $Ph^-{\cdot}H_2O$ curve (red). The inset shows both curves in the magnified T range that includes the observed 520 K temperature of $Ph^-{\cdot}(H_2O)_2$ and the 560 K temperature of $Ph^-{\cdot}H_2O$. The shaded guides indicate the ±10 K confidence intervals of the T determinations and the resulting RTE fractions uncertainties. We conclude that the RTE fraction of $Ph^-{\cdot}(H_2O)_2$ at its T = 520 K is similar to that of $Ph^-{\cdot}H_2O$ at its T = 560 K: both are approximately 1×10^{-4}. That is, the evaporative cooling of $Ph^-{\cdot}(H_2O)_2$ or $Ph^-{\cdot}H_2O$ stops when the probability of ejecting a water molecule, i.e., the evaporation rate, decreases to the same small value. Extending this approach, we can also predict that the terminal temperature of $Ph^-{\cdot}(H_2O)_3$ (not studied here) will be about 500-505 K.

5. Conclusions

Microscopic solvation sets an upper bound on the temperature of stable clusters. The limiting temperature is determined by the maximum excitation that the solvation interactions can sustain without significant solvent evaporation occurring on the timescale of the experiment. The excita-

tion limit is set by the solvent binding energy and the density of states associated with the intermolecular degrees of freedom of the cluster. Therefore, the upper temperature is an intrinsic property of the cluster species, i.e., its characteristic solvation temperature. The terminal temperature of clusters from a hot ion source will always be close to CST, and only if the source temperature is lower than CST will the observed temperature be determined by the source conditions.

Thermal excitation alters the spectroscopic signatures of the solvated ions and affects their interactions with neighboring molecules. By analyzing their spectra, the temperatures of the $Ph^-{\cdot}H_2O$ and $Ph^-{\cdot}(H_2O)_2$ cluster ions were found to be 560 K and 520 K, respectively, compared to 700 K for Ph^- from the same ion source. Compared to the theory predictions for cold clusters, high temperature of the environment significantly reduces the hydration stabilization of the ions and the corresponding band shifts in their spectra. These results are consistent with a statistical model that quantifies the average energy content of the intermolecular degrees of freedom of the cluster, $\langle E_{IM} \rangle$. The model supports the conclusion that the observed temperatures represent the intrinsic properties of $Ph^-{\cdot}H_2O$ and $Ph^-{\cdot}(H_2O)_2$. The conclusions can be generalized as an empirical rule for estimating the characteristic limit of cluster temperature: a cluster's CST is defined approximately by the inflection point on its $\langle E_{IM} \rangle$ vs. T curve (for example, see Figure 8).

ASSOCIATED CONTENT

Supporting Information

The Supporting Information is available free of charge at https://pubs.acs.org/doi/xxxxxxxxxx.

Equilibrium geometries of Ph^- and $Ph^-{\cdot}H_2O$, normal modes of $Ph^-{\cdot}H_2O$, Ph^-, and H_2O, and discussion of vibrational energy partitioning for dissociative detachment transitions (PDF)

AUTHOR INFORMATION

ORCID

Beverly Feng (formerly Beverly Ru): 0000-0003-1258-6224

Andrei Sanov: 0000-0002-2373-4387

Author Contributions

The manuscript was written through contributions of all authors. All authors have given approval to the final version of the manuscript.

Notes

The authors declare no competing financial interest.

ACKNOWLEDGMENT

Financial support of this work was provided by the U.S. National Science Foundation through grant CHE-2153986.

References

1. Millar, T. J.; Walsh, C.; Field, T. A., Negative Ions in Space. *Chem. Rev.* **2017,** *117*, 1765-1795.
2. Wakelam, V.; Herbst, E., Polycyclic Aromatic Hydrocarbons in Dense Cloud Chemistry. *Astrophys. J.* **2008,** *680*, 371-383.
3. Kaiser, R. I.; Hansen, N., An Aromatic Universe–A Physical Chemistry Perspective. *J. Phys. Chem. A* **2021,** *125*, 3826-3840.
4. Mansurov, Z. A., Soot Formation in Combustion Processes. *Combust., Explos. Shock Waves (Engl. Transl.)* **2005,** *41*, 727-744.
5. Parker, D. S. N.; Kaiser, R. I.; Troy, T. P.; Kostko, O.; Ahmed, M.; Mebel, A. M., Toward the Oxidation of the Phenyl Radical and Prevention of PAH Formation in Combustion Systems. *J. Phys. Chem. A* **2015,** *119*, 7145-7154.
6. Gunion, R. F.; Gilles, M. K.; Polak, M. L.; Lineberger, W. C., Ultraviolet Photoelectron-Spectroscopy of the Phenide, Benzyl and Phenoxide Anions, with ab initio Calculations. *Int. J. Mass Spectrom.* **1992,** *117*, 601-620.
7. Ru, B.; Sanov, A., Photoelectron Spectra of Hot Polyatomic Ions: A Statistical Treatment of Phenide. *J. Phys. Chem. A* **2022,** *126*, 9423-9439.
8. McQuarrie, D. A., *Statistical Mechanics*. University Science Books: Sausalito, California, 2000.
9. Gilbert, R. G.; Smith, S. C., *Theory of unimolecular and recombination reactions*. Blackwell Scientific Publications: Oxford, England, 1990.
10. Hill, T. L., *An Introduction to Statistical Thermodynamics*. Dover Publications: New York, 2012.
11. Sivaranjana Reddy, V.; Venkatesan, T. S.; Mahapatra, S., Vibronic interactions in the photodetachment spectroscopy of phenide anion. *J. Chem. Phys.* **2007,** *126*, 074306.
12. Franck, J.; Dymond, E. G., Elementary processes of photochemical reactions. *Trans. Faraday Soc.* **1926,** *21*, 536-542.
13. Condon, E., A Theory of Intensity Distribution in Band Systems. *Phys. Rev.* **1926,** *28*, 1182-1201.
14. Condon, E. U., The Franck-Condon Principle and Related Topics. *Am. J. Phys.* **1947,** *15*, 365-374.
15. Ayotte, P.; Weddle, G. H.; Kim, J.; Johnson, M. A., Vibrational Spectroscopy of the Ionic Hydrogen Bond: Fermi Resonances and Ion−Molecule Stretching Frequencies in the Binary $X^-\cdot H_2O$ (X = Cl, Br, I) Complexes via Argon Predissociation Spectroscopy. *J. Am. Chem. Soc.* **1998,** *120*, 12361-12362.
16. Ayotte, P.; Weddle, G. H.; Kim, J.; Johnson, M. A., Mass-selected "matrix isolation" infrared spectroscopy of the $I^-\cdot(H_2O)_2$ complex: making and breaking the inter-water hydrogen-bond. *Chem. Phys.* **1998,** *239*, 485-491.
17. Elliott, B. M.; Relph, R. A.; Roscioli, J. R.; Bopp, J. C.; Gardenier, G. H.; Guasco, T. L.; Johnson, M. A., Isolating the spectra of cluster ion isomers using Ar-"tag"-mediated IR-IR double resonance within the vibrational manifolds: Application to $NO_2^-\cdot H_2O$. *J. Chem. Phys.* **2008,** *129*, 094303.
18. Gerardi, H.; Deblase, A.; Su, X.; Jordan, K.; McCoy, A. B.; Johnson, M., Unraveling the Anomalous Solvatochromic Response of the Formate Ion Vibrational Spectrum: An Infrared,

Ar-Tagging Study of the HCO_2^-, DCO_2^-, and $HCO_2^-\cdot H_2O$ Ions. *J. Phys. Chem. Lett.* **2011,** *2*, 2437.
19. Punyain, W.; Takahashi, K., Evaluation of Ar tagging toward the vibrational spectra and zero point energy of X^-HOH, X^-DOH, and X^-HOD, for X = F, Cl, Br. *Phys. Chem. Chem. Phys.* **2021,** *23*, 9492-9499.
20. Diken, E. G.; Robertson, W. H.; Johnson, M. A., The Vibrational Spectrum of the Neutral $(H_2O)_6$ Precursor to the "Magic" $(H_2O)_6^-$ Cluster Anion by Argon-Mediated, Population-Modulated Electron Attachment Spectroscopy. *J. Phys. Chem. A* **2004,** *108*, 64-68.
21. Weber, J. M.; Kelley, J. A.; Robertson, W. H.; Johnson, M. A., Hydration of a structured excess charge distribution: Infrared spectroscopy of the $O_2^-\cdot(H_2O)_n$, $(1 \le n \le 5)$ clusters. *J. Chem. Phys.* **2001,** *114*, 2698-2706.
22. Kelley, J. A.; Weber, J. M.; Lisle, K. M.; Robertson, W. H.; Ayotte, P.; Johnson, M. A., The infrared predissociation spectra of $Cl^-\cdot H_2O\cdot Ar_n$ (n = 1-5): experimental determination of the influence of Ar solvent atoms. *Chem. Phys. Lett.* **2000,** *327*, 1-6.
23. Okumura, M.; Yeh, L. I.; Myers, J. D.; Lee, Y. T., Infrared spectra of the cluster ions $H_7O_3^+\cdot H_2$ and $H_9O_4^+\cdot H_2$. *J Chem Phys* **1986,** *85*, 2328-2329.
24. Jarrold, C. C., Probing Anion–Molecule Complexes of Atmospheric Relevance Using Anion Photoelectron Detachment Spectroscopy. *ACS Phys. Chem. Au* **2023,** *3*, 17-29.
25. Klots, C. E., Evaporative cooling. *J. Chem. Phys.* **1985,** *83*, 5854.
26. Klots, C. E., Temperatures of evaporating clusters. *Nature* **1987,** *327*, 222-223.
27. Klots, C. E., The evaporative ensemble. *Z. Phys. D: At., Mol. Clusters* **1987,** *5*, 83-89.
28. Klots, C. E., Thermal kinetics in small systems. *J. Chem. Phys.* **1989,** *90*, 4470-4472.
29. Engelking, P. C., Determination of cluster binding energy from evaporative lifetime and average kinetic energy release: application to $(CO_2)_n^+$ and Ar_n^+ clusters. *J. Chem. Phys.* **1987,** *87*, 936-40.
30. Wester, R.; Davis, A. V.; Bragg, A. E.; Neumark, D. M., Cluster calorimetry by femtosecond stimulated emission pumping: Excitation and evaporative cooling of $I_2^-(CO_2)_n$. *Phys. Rev. A* **2002,** *65*, 051201.
31. Surber, E.; Sanov, A., Photoelectron imaging spectroscopy of molecular and cluster anions: CS_2^- and $OCS^-(H_2O)_{1,2}$. *J. Chem. Phys.* **2002,** *116*, 5921-5924.
32. Mabbs, R.; Surber, E.; Sanov, A., Photoelectron Imaging of Negative Ions: Atomic Anions to Molecular Clusters. *Analyst* **2003,** *128*, 765-772.
33. Johnson, M. A.; Lineberger, W. C., Pulsed Methods for Cluster Ion Spectroscopy. In *Techniques for the Study of Ion Molecule Reactions*, Farrar, J. M.; Saunders, W. H., Eds. Wiley: New York, 1988; pp 591-635.
34. Nadal, M. E.; Kleiber, P. D.; Lineberger, W. C., Photofragmentation of Mass-Selected $ICl^-(CO_2)_n$ Cluster Ions: Solvation Effects on the Structure and Dynamics of the Ionic Chromophore. *J. Chem. Phys.* **1996,** *105*, 504-514.
35. Surber, E.; Ananthavel, S. P.; Sanov, A., Nonexistent electron affinity of OCS and the stabilization of carbonyl sulfide anions by gas phase hydration. *J. Chem. Phys.* **2002,** *116*, 1920-1929.
36. Blackstone, C. C. Exploring the Chemistry of Methoxide with Oxygen Through Photoelectron Imaging Spectroscopy. Ph.D. dissertation, University of Arizona, Tucson, 2020.
37. Wiley, W. C.; McLaren, I. H., Time-of-Flight Mass Spectrometer with Improved Resolution. *Rev. Sci. Instrum.* **1955,** *26*, 1150.

38. Eppink, A. T. J. B.; Parker, D. H., Velocity map imaging of ions and electrons using electrostatic lenses: Application in photoelectron and photofragment ion imaging of molecular oxygen. *Rev. Sci. Instrum.* **1997,** *68*, 3477-3484.
39. Chandler, D. W.; Houston, P. L., Two-Dimensional Imaging of State-Selected Photodissociation Products Detected by Multiphoton Ionization. *J. Chem. Phys.* **1987,** *87*, 1445-1447.
40. Heck, A. J. R.; Chandler, D. W., Imaging Techniques For the Study of Chemical Reaction Dynamics. *Annu. Rev. Phys. Chem.* **1995,** *46*, 335-372.
41. Dribinski, V.; Ossadtchi, A.; Mandelshtam, V. A.; Reisler, H., Reconstruction of abel-transformable images: The Gaussian basis-set expansion abel transform method. *Rev. Sci. Instrum.* **2002,** *73*, 2634-2642.
42. Gozem, S.; Krylov, A. I., The ezSpectra suite: An easy-to-use toolkit for spectroscopy modeling. *Wiley Interdiscip. Rev.: Comput. Mol. Sci.* **2021,** *12*, e1546.
43. Engelking, P. C., Strong electron-dipole coupling in photodetachment of molecular negative ions: Anomalous rotational thresholds. *Phys. Rev. A* **1982,** *26*, 740-745.
44. Lakhmanskaya, O.; Simpson, M.; Murauer, S.; Kokoouline, V.; Wester, R., Photodetachment spectroscopy of cold trapped NH_2^- near threshold. *J. Chem. Phys.* **2018,** *149*, 104302.
45. Simpson, M.; Nötzold, M.; Schmidt-May, A.; Michaelsen, T.; Bastian, B.; Meyer, J.; Wild, R.; Gianturco, F. A.; Milovanović, M.; Kokoouline, V., et al., Threshold photodetachment spectroscopy of the astrochemical anion CN^-. *J. Chem. Phys.* **2020,** *153*, 184309.
46. Dauletyarov, Y.; Ru, B.; Sanov, A., Anion of Oxalyl Chloride: Structure and Spectroscopy. *J. Phys. Chem. A* **2021,** *125*, 9865-9876.
47. Wigner, E. P., On the behavior of cross sections near thresholds. *Phys. Rev.* **1948,** *73*, 1002-1009.
48. Ru, B.; Hart, C. A.; Mabbs, R.; Gozem, S.; Krylov, A. I.; Sanov, A., Dipole effects in the photoelectron angular distributions of the sulfur monoxide anion. *Phys. Chem. Chem. Phys.* **2022,** *24*, 23367-23381.
49. Shao, Y. H.; Gan, Z. T.; Epifanovsky, E.; Gilbert, A. T. B.; Wormit, M.; Kussmann, J.; Lange, A. W.; Behn, A.; Deng, J.; Feng, X. T., et al., Advances in molecular quantum chemistry contained in the Q-Chem 4 program package. *Mol. Phys.* **2015,** *113*, 184-215.
50. Dauletyarov, Y.; Sanov, A., Weak covalent interactions and anionic charge-sharing polymerisation in cluster environments. *Phys. Chem. Chem. Phys.* **2021,** *23*, 11596-11610.
51. Boys, S. F.; Bernardi, F., Calculation of Small Molecular Interactions by Differences of Separate Total Energies. Some Procedures with Reduced Errors. *Mol. Phys.* **1970,** *19*, 553-566.
52. Grebowsky, J. M.; McKelvey, J. P., Density-of-States Function for the Harmonic Oscillator: A Simple and Direct Approach. *Am. J. Phys.* **1967,** *35*, 352-353.
53. Terletskii, Y. P., *Statistical Physics*. North-Holland Publishing Company: Amsterdam, 1971.
54. Angelova, M.; Frank, A., Algebraic Model of Molecular Thermodunamics. In *Quantum Theory and Symmetries*, World Scientific: 2002; pp 243-248.

Table 1. Parameter values used to produce the model spectra shown in Figure 3 in red.

Species	T / K	Wigner exponent	Hydration shift / eV
Ph^-	700(10)	0.50	0
$Ph^-{\cdot}H_2O$	560(10)	0.45	0.38(1)
$Ph^-{\cdot}(H_2O)_2$	520(10)	0.10	0.63(1)

Figure 1

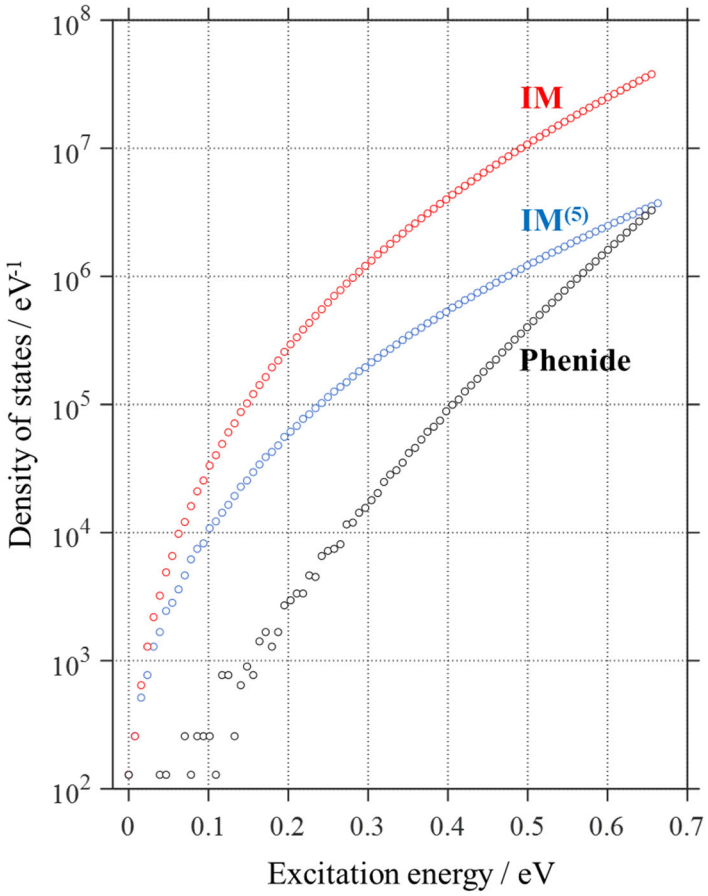

Figure 1. The density of states spanned by the 27 internal vibrational modes of phenide in the $Ph^{-}\cdot H_2O$ cluster (black symbols), all six IM modes (red symbols), and the 5 dissociative IM modes only (blue symbols) plotted with respect to the respective excitation energies (excluding ZPE).

Figure 2

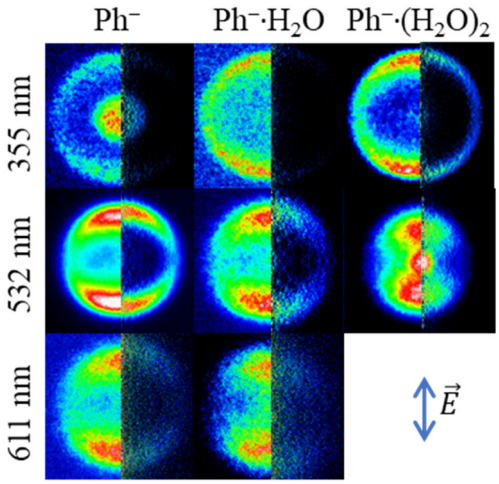

Figure 2. Raw photoelectron images (left halves) and inverse Abel transformation (right halves) of Ph^- and $Ph^-\cdot(H_2O)_{1,2}$ obtained at the indicated laser wavelength. The light polarization direction is indicated in the bottom-right corner.

Figure 3

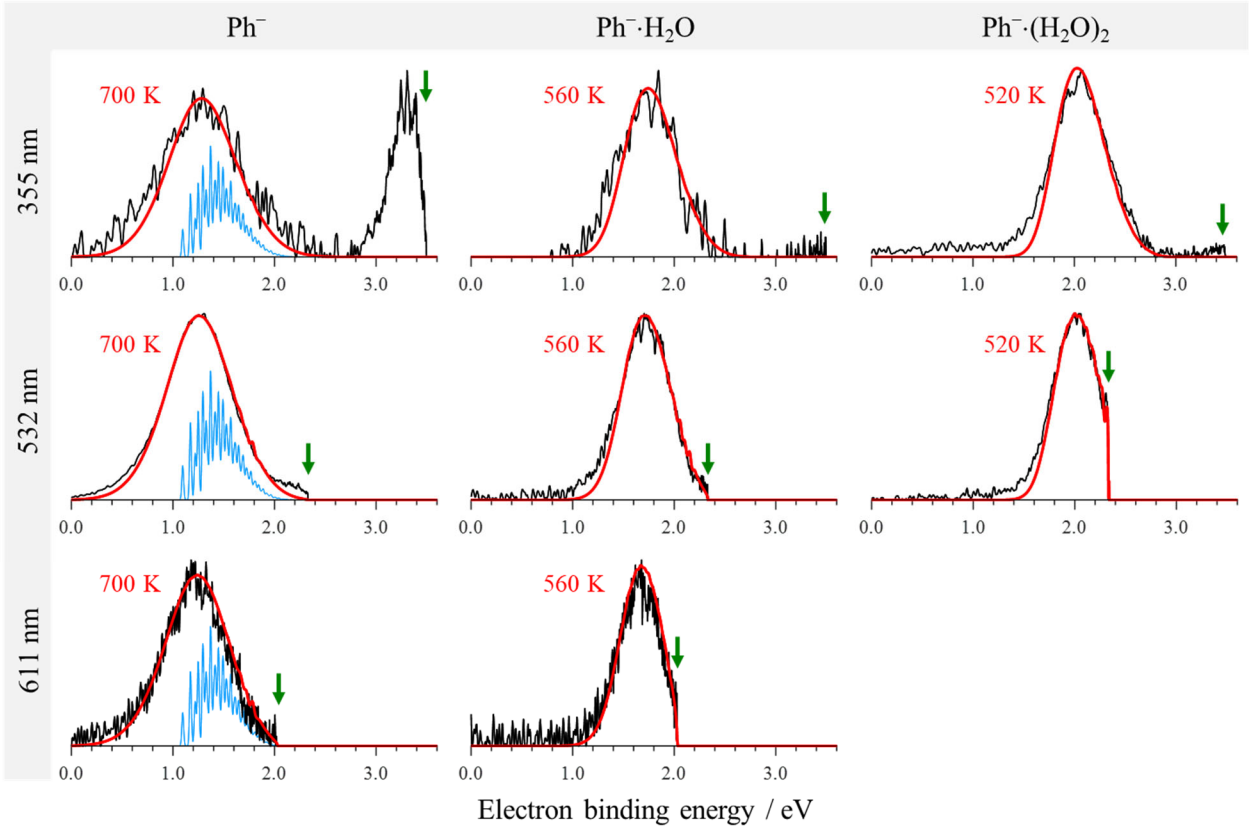

Figure 3. Photoelectron spectra of Ph^- and $Ph^-\cdot(H_2O)_{1,2}$ for the laser wavelength indicated. The black lines represent the experimental data extracted from the images in Figure 2. The red lines are the model spectra obtained at the temperatures indicated in each panel, used to determine the experimental temperatures of the ions. Model details are described in the text and the relevant model parameters are summarized in Table 1. The blue lines in the Ph^- column represent the corresponding cold FC simulations, also described in the text. The green vertical arrows indicate the energetic limit for each spectrum corresponding to eBE = $h\nu$.

Figure 4

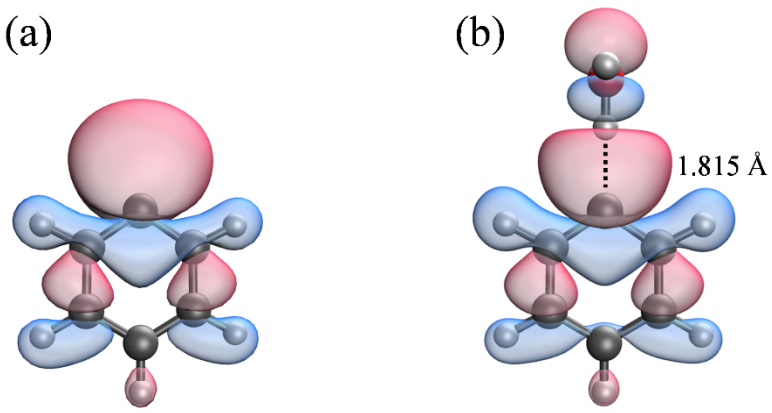

Figure 4. (a) Phenide and (b) $Ph^{-}{\cdot}H_2O$ equilibrium structures optimized at the CCSD level of theory with the aug-cc-pVDZ basis set. All geometric parameters (in the form of the corresponding Z-matrices) as well as vibrational frequencies are given in SI. The Hartree-Fock HOMOs of both species are also shown using the iso-values of 0.05.

Figure 5

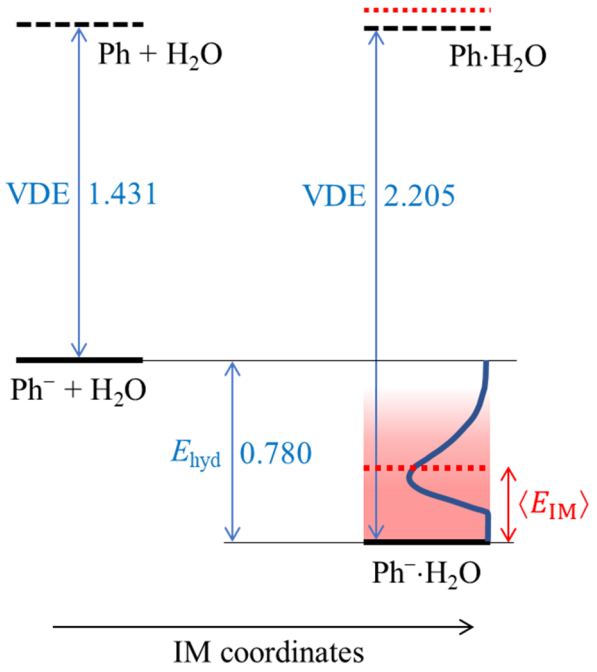

Figure 5. A schematic energy diagram comparing the photodetachment of Ph^- and $Ph^-{\cdot}H_2O$. Thermal distribution with respect to IM degrees of freedom (only) is included on the right.

Figure 6

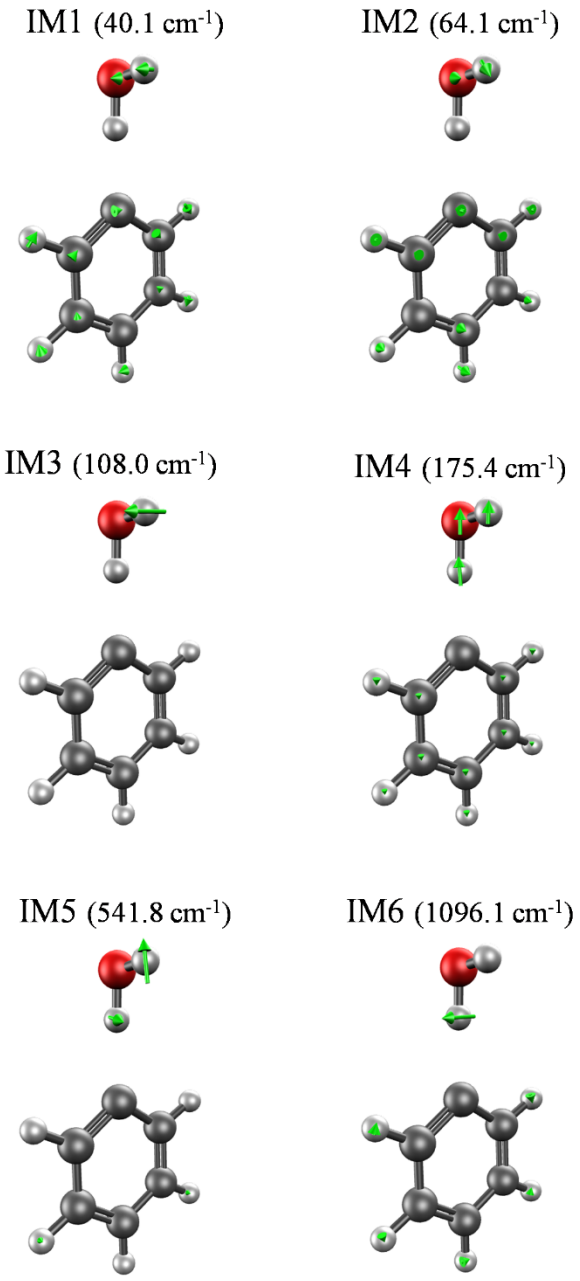

Figure 6. The $Ph^{-}\cdot H_2O$ vibrational modes corresponding predominantly to the phenide-water motions, labeled IM1-IM6. A complete set of all 36 vibrational frequencies of the cluster is given in Table S1 in SI.

Figure 7

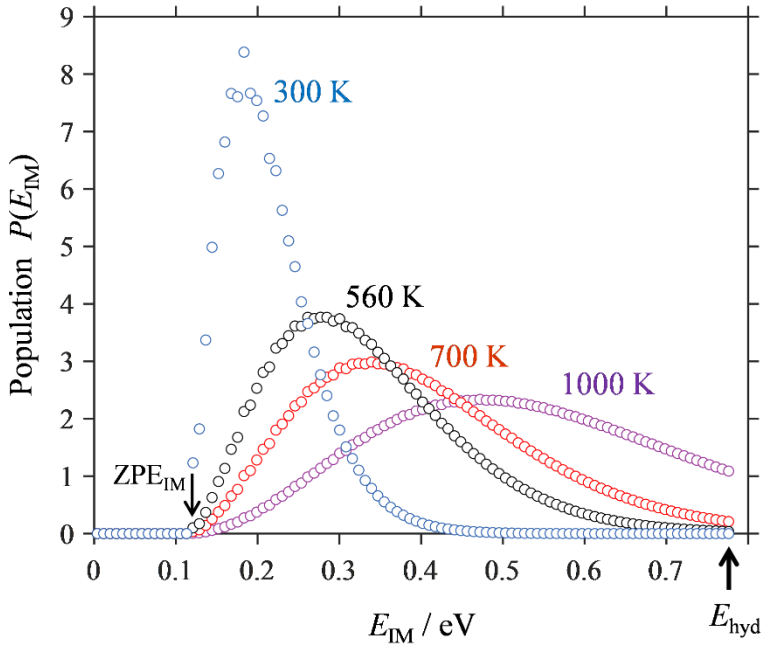

Figure 7. The thermal energy distributions for the six IM modes of $Ph^{-}\cdot H_2O$ calculated at four different temperatures using the IM-subspace DOS and eqn 1.

Figure 8

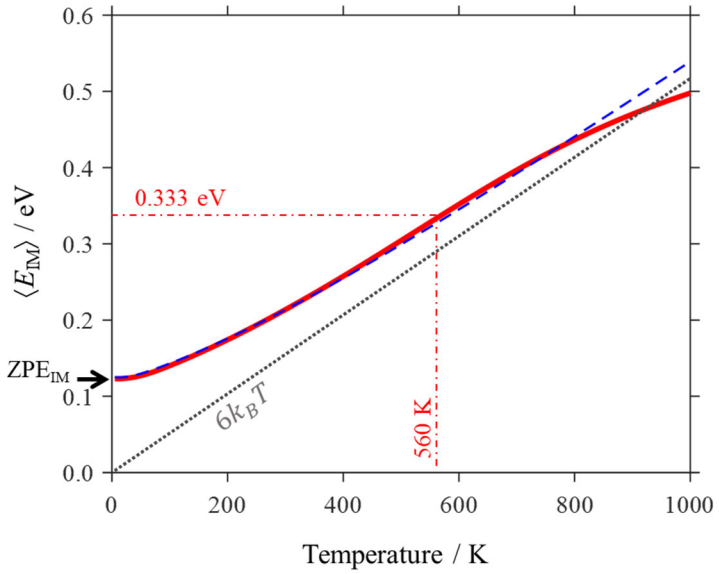

Figure 8. Red solid curve: the ensemble average of IM energy in $Ph^{-}{\cdot}H_2O$ calculated as a function of temperature using eqn 2. Blue dashed curve: same but treating all six IM modes in the harmonic approximation (i.e., no dissociation allowed). Black dotted line: $\langle E_{\mathrm{IM}} \rangle = 6k_BT$ predicted by the equipartition theorem for the classical harmonic limit. The dash-dotted guides indicate the 560 K spectroscopic temperature of $Ph^{-}{\cdot}H_2O$ and the corresponding IM energy, $\langle E_{\mathrm{IM}} \rangle$ = 0.333 eV.

Figure 9

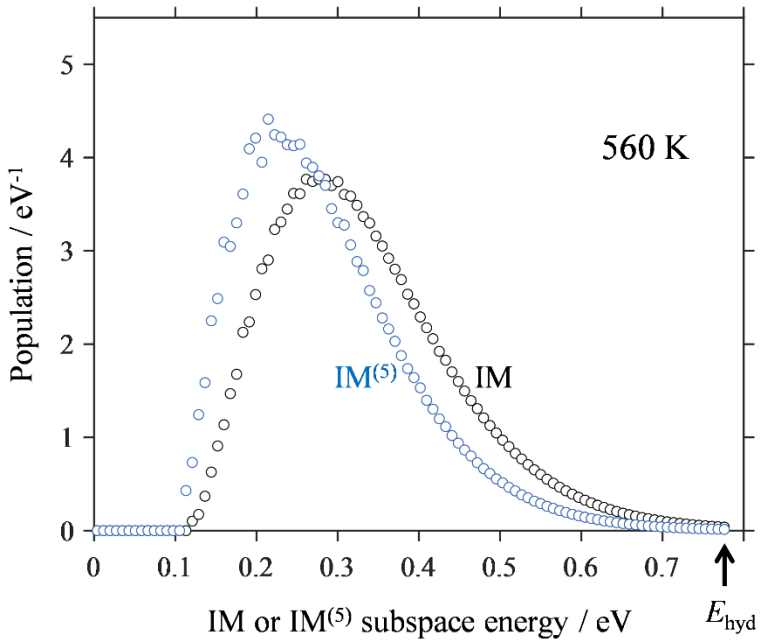

Figure 9. The $T = 560$ K energy distributions for the five dissociative IM modes of $Ph^{-}\cdot H_2O$, $IM^{(5)}$ (blue symbols). The corresponding six-dimensional IM-space distribution (black symbols) is reproduced from Figure 7 for comparison.

Figure 10

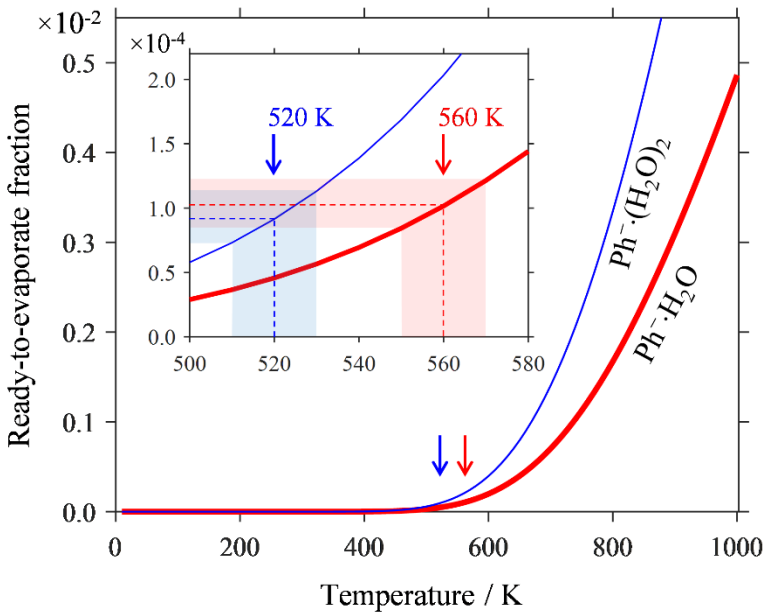

Figure 10. Red curve: the temperature-dependent "ready-to-dissociate" fraction of $Ph^{-}\cdot H_2O$, RTE = $f_{1\%}(T)$, as defined in the text. Blue curve: same for $Ph^{-}\cdot(H_2O)_2$, RTE = $2f_{1\%}(T)$. The inset shows a magnified portion of both curves in the T range that includes the 520 K experimental temperature of $Ph^{-}\cdot(H_2O)_2$ and the 560 K temperature of $Ph^{-}\cdot H_2O$. The shaded guides indicate the ±10 K confidence intervals of the T determinations and the resulting uncertainties of the RTE fractions.

TOC graphic